The EMBO Journal (2006) 25, 3245–3256 | © 2006 European Molecular Biology Organization | All Rights Reserved 0261-4189/06
www.embojournal.org

THE EMBO JOURNAL

Dynamic molecular confinement in the plasma membrane by microdomains and the cytoskeleton meshwork

Pierre-François Lenne[1,2,7], Laure Wawrezinieck[1,2,3,4,5,7], Fabien Conchonaud[3,4,5], Olivier Wurtz[3,4,5,8], Annie Boned[3,4,5], Xiao-Jun Guo[3,4,5,6], Hervé Rigneault[1,2], Hai-Tao He[3,4,5] and Didier Marguet[3,4,5,*]

[1]Institut Fresnel, Université Paul Cézanne, Marseille, France, [2]CNRS UMR 6133, Marseille, France, [3]Centre d'Immunologie de Marseille-Luminy, Université de la Méditerranée, Marseille, France, [4]INSERM, UMR 631, Marseille, France, [5]CNRS, UMR 6102, Marseille, France and [6]Laboratoire de Biochimie et Physicochimie des Membranes Biologiques, Université Paul Cézanne, Marseille, France

It is by now widely recognized that cell membranes show complex patterns of lateral organization. Two mechanisms involving either a lipid-dependent (microdomain model) or cytoskeleton-based (meshwork model) process are thought to be responsible for these plasma membrane organizations. In the present study, fluorescence correlation spectroscopy measurements on various spatial scales were performed in order to directly identify and characterize these two processes in live cells with a high temporal resolution, without any loss of spatial information. Putative raft markers were found to be dynamically compartmented within tens of milliseconds into small microdomains ($\varnothing < 120$ nm) that are sensitive to the cholesterol and sphingomyelin levels, whereas actin-based cytoskeleton barriers are responsible for the confinement of the transferrin receptor protein. A free-like diffusion was observed when both the lipid-dependent and cytoskeleton-based organizations were disrupted, which suggests that these are two main compartmentalizing forces at work in the plasma membrane.

The EMBO Journal (2006) **25,** 3245–3256. doi:10.1038/sj.emboj.7601214; Published online 6 July 2006
Subject Categories: membranes & transport
Keywords: actin meshwork; confined diffusion; fluorescence correlation spectroscopy; lipid rafts; membrane microdomain

Introduction

Although it is generally assumed that lateral heterogeneities exist in cell membranes (Edidin, 2003; Simons and Vaz, 2004), the factors responsible for the local organization of the plasma membrane are poorly understood. Various mechanisms have been suggested to explain the significant discrepancies observed in the diffusion rates of lipids and proteins between artificial membranes and plasma membranes. For instance, membrane protein diffusion differs from pure Brownian diffusion because of the transient interactions occurring with large multimeric complexes (Marguet *et al*, 1999), the obstacles resulting from direct and indirect molecular immobilization (Sako and Kusumi, 1994; Fujiwara *et al*, 2002), and the corrals formed on various submicrometric scales (Yechiel and Edidin, 1987). There is still some controversy about the ability of lipids to form domains, which are also known as lipid rafts, in plasma membranes (Simons and Ikonen, 1997; Brown and London, 1998; Edidin, 2003; Munro, 2003; Simons and Vaz, 2004; van Meer, 2005; Marguet *et al*, 2006). In these lipid domains, cholesterol is thought to be tightly packed with long saturated fatty acid chains of specific glycosphingolipids, thus favoring lipid phase separation processes. It has been suggested that these domains may be insoluble in nonionic detergents (Brown and London, 1998; Drevot *et al*, 2002). In addition to studies characterizing biochemical rafts, morphological approaches have been used to prove the existence of these rafts in cell membranes, but the conclusions drawn have been rather controversial, since the results depended strongly on the methods used. When the lateral motion of lipid probes was analyzed using single dye tracing methods, the domain size was found to range from 0.2 to 2 μm (Schutz *et al*, 2000). These data are in the same range as those obtained on the barrier-free paths of membrane proteins, but the latter depend mainly on how the cytoskeleton is organized (Sako and Kusumi, 1994). Other studies using biophysical approaches on live cells have strongly supported the idea that rafts are small diffusive entities (Pralle *et al*, 2000; Sharma *et al*, 2004). Fluorescence resonance energy transfer methods (FRET) have been used to probe the molecular aggregates present in lipid rafts. Experiments of this kind using different lipid-modified proteins expressed in the apical membrane of MDCK cells have led to divergent conclusions (Kenworthy and Edidin, 1998; Zacharias *et al*, 2002; Hess *et al*, 2005). FRAP measurements on live cells have provided evidence that the anchoring mode determines the protein–raft interaction dynamics (Shvartsman *et al*, 2003). A direct visualization of liquid-ordered domains was recently obtained using fluorescent cell staining procedures, although information is still lacking about the dynamic aspects of these structures (Gaus *et al*, 2003). In fact, these methods span different spatiotemporal scales, and the data obtained about the features of rafts, and even their existence in live cells, may therefore not always seem to be in agreement.

Improving our knowledge of membrane organization requires developing new methods in which the temporal resolution is improved without any loss of spatial information. For instance, FRAP measurements performed on different

*Corresponding author. Centre d'Immunologie de Marseille Luminy, CNRS, Parc Scientifique de Luminy, Case 906, 13288 Marseille Cedex 13009, France. Tel.: +33 491 269 128; Fax: +33 491 269 430; E-mail: marguet@ciml.univ-mrs.fr
[7]These authors contributed equally to this work
[8]Present address: Université de Rouen, INSERM U413, Mont Saint Aignan, France

Received: 9 February 2006; accepted: 6 June 2006; published online: 6 July 2006

spatial scales have made it possible to identify micrometer-scale domains present in the plasma membrane of fibroblasts (Yechiel and Edidin, 1987). By applying a similar strategy using fluorescence correlation spectroscopy (FCS) methods, we recently managed to distinguish between different submicron confinement models. In the latter study, we described a novel method of performing FCS on various observation scales (Wawrezinieck *et al*, 2004) and developed a simple analytical method of investigating the complexity of the cell membrane organization and the dynamic processes involved (Wawrezinieck *et al*, 2005). This novel method could be used to identify and discriminate between variously organized submicroscopic domains preventing the free lateral diffusion of membrane components (Saxton, 2005). The *FCS Diffusion Law* was defined in the latter study as the plot of the diffusion time (i.e. the average time a fluorescent molecule stays within the illuminated area) versus the observation area. Based on extensive confined diffusion modeling studies, it was established that the *y*-intercept t_0 in the graph of the FCS diffusion laws is positive in the case of confining in microdomains (dynamic partitioning into microdomains) but negative in that of trapping in a meshwork (actin-based cytoskeleton corrals).

Here, it was proposed to investigate the dynamics of membrane organization in live cells. The diffusion behavior of various membrane components was described and it was established whether molecular confinement depends on the specific cholesterol/sphingomyelin membrane content or on the presence of actin-based cytoskeleton barriers.

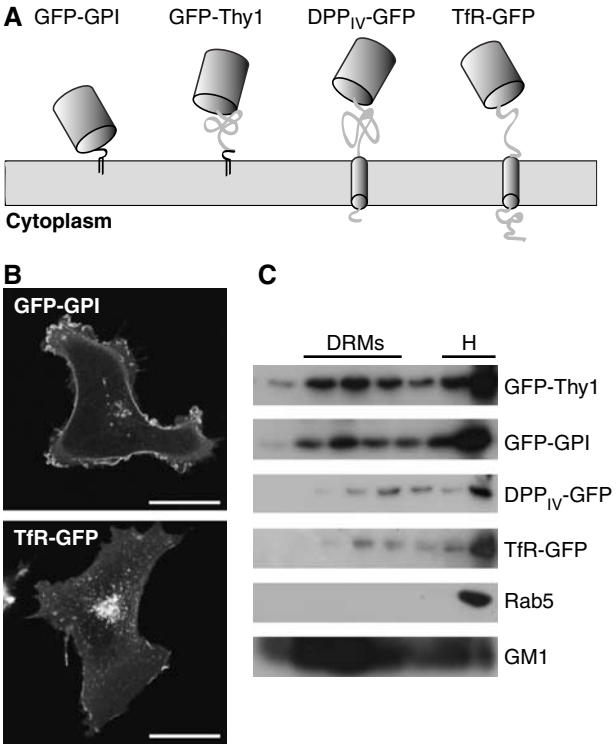

Figure 1 GFP-tagged proteins used in this study. (**A**) Membrane topology of the GFP-tagged proteins. (**B**) Confocal images of COS-7 cells expressing the GFP-GPI and TfR-GFP proteins. Scale bar is 20 μm. (**C**) Brij 98 solubilized PNS from transfected COS-7 cells was fractionated on the sucrose gradient and blotted with anti-GFP, anti-Rab 5 antibodies or cholera toxin B.

Results

Molecules used to establish the presence of domains in plasma membranes

To establish the presence of domains in the plasma membrane, the diffusion behavior of four different groups of membrane components was investigated: (1) a glycerophospholipid group with two fluorescent lipid analogs, BODIPY-C_5-phosphatidylcholine (FL-PC) and BODIPY-dihexadecanoyl-phospho-ethanolamine (FL-PE), (2) a sphingolipid group including the BODIPY-C_5-sphingomyelin (FL-SM) and BODIPY-C_5-ganglioside-G_{M1} (FL-G_{M1}) analogs, (3) a glycosylphosphatidylinositol (GPI)-anchored protein group in which the GFP was either tagged onto the GPI-anchoring signal originating from the decay accelerating factor (GFP-GPI) or inserted just after the signal peptide of Thy1 (GFP-Thy1), and (4) a GFP-tagged transmembrane protein group including the dipeptidyl peptidase IV (DPP$_{IV}$-GFP) and the transferrin receptor (TfR-GFP) (Figure 1A).

To examine the mobility of lipid analogs, COS-7 cells were labeled using the lipid exchange method (Martin and Pagano, 1994). Laser scanning confocal microscopy showed that the probes were uniformly distributed in the plasma membrane. A vesicular staining pattern consisting of small intracellular dots was also observed (Figure 2A–C). All the GFP-tagged proteins were efficiently addressed to the plasma membrane when transiently expressed in COS-7 cells (Figure 1B and data not shown). Vesicular staining was also detected in the cytosol, especially in the perinuclear area.

Based on previous studies, these molecules are known to be either present in high levels or depleted from detergent resistant membranes (DRMs). This was confirmed by Brij 98 detergent-insolubility experiments performed at physiological temperatures (Drevot *et al*, 2002). Although the BODIPY fluorophore can affect the properties of lipids, yielding analogs with quite different characteristics from those of their natural counterparts (Kuerschner *et al*, 2005), both FL-G_{M1} and FL-SM were readily detected in DRMs, where they accounted for 11 and 17% of the total fluorescence, respectively. This association is not negligible, since under the same experimental conditions, about 20% of the GFP-Thy1 or GFP-GPI molecules were detected in DRMs, whereas those anchored by a classical transmembrane peptide were barely detectable (Figure 1C).

The different groups of membrane components follow distinct FCS diffusion laws

As described previously, the *FCS diffusion law* giving the diffusion time τ_d (i.e. the average time a fluorescent molecule stays within the illuminated area) versus the beam area, where w denotes the beam radius, should provide a suitable analytical method for determining the diffusion behavior of a molecule in the membrane (Saxton, 2005; Wawrezinieck *et al*, 2005). This approach is based on the fact that if molecules diffuse freely, one can expect to obtain a linear function between τ_d and w^2: the curve $\tau_d = f(w^2)$ will intercept the time origin and its slope will correspond to the diffusion coefficient D in this environment. In most situations where diffusion is hindered, the FCS diffusion law will no longer fit this scheme. By sizing the laser beam filling the microscope objective, we varied w experimentally from 200

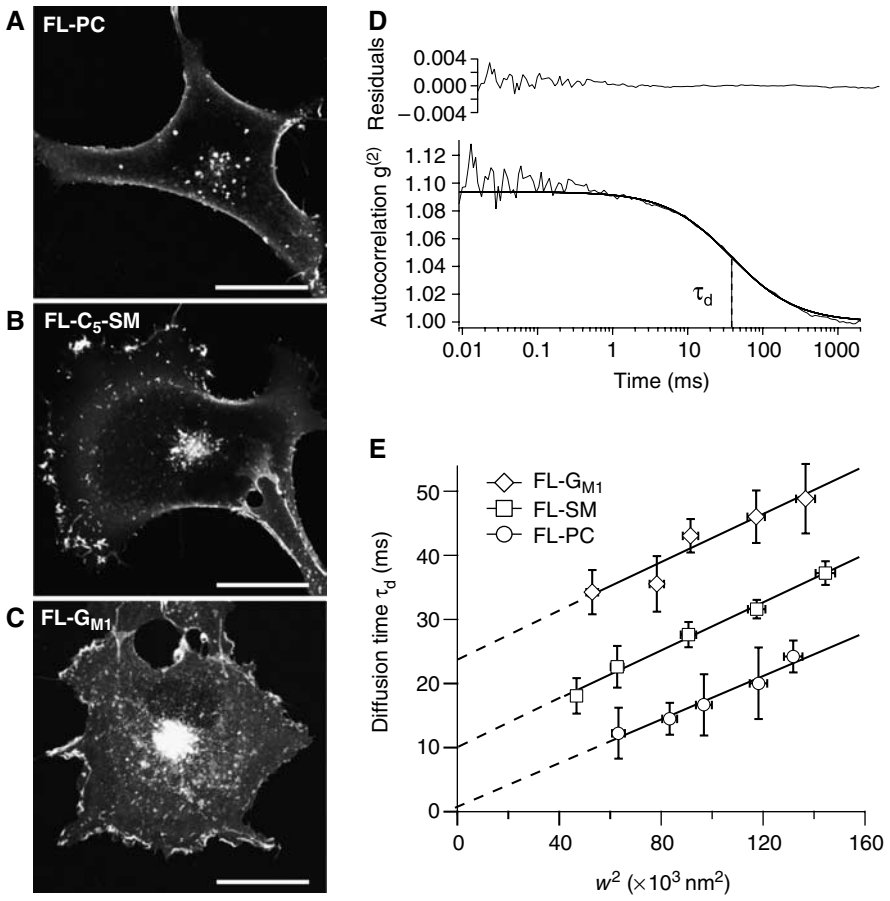

Figure 2 Diffusion behavior of lipid analogs. Confocal images of COS-7 cells after labeling with lipid analogs: (**A**) FL-PC, (**B**) FL-SM and (**C**) FL-G_{M1}. Scale bar is 20 μm. (**D**) ACF obtained with FL-G_{M1} lipids. The curve was satisfactorily fitted with a 1-species free diffusion model (see Supplementary data). The diffusion time τ_d was given by the lag time at half maximum. (**E**) Diffusion behavior of lipid analogs. Confinement times were determined from the position at which the diffusion curves and the time-axis intersected. Error bars in *x* and *y* give standard deviations (s.d.) of the means.

to 400 nm; the lower limit was imposed by the diffraction law, whereas the upper one was based on a compromise between the spatial resolution and FCS constraints.

We first investigated the lipid dynamics using trace mole fractions of probes relative to the total lipids in order to minimize any membrane perturbations. Based on experimental autocorrelation functions (ACF), the data were efficiently fitted using a single component, giving a single decay time (see Supplementary data and Figure 2D). In this case, τ_d was obtained by measuring the lag time at half the maximum ACF value. With all the lipid probes used, τ_d increased linearly with w^2 but the intersections with the time axis differed (Figure 2E). In the case of the glycerophospholipid analogs FL-PC and FL-PE, the FCS diffusion laws intercepted the time axis at the origin at almost null t_0 values (-0.4 ± 0.8 and 0.2 ± 0.7 ms, respectively). By contrast, t_0 was strictly positive in the case of the sphingolipid analogs FL-G_{M1}, FL-C_5-SM and FL-C_{12}-SM, where values of 24.3 ± 1.9, 10.2 ± 0.6 and 9.7 ± 0.5 ms were obtained, respectively.

With all the chimeric proteins used, two decay times were clearly identified from the ACFs (Figure 3A–B and data not shown): a short time τ_{fast} and a longer one τ_d. We checked that the slow decay time corresponded to the diffusion time of plasma membrane-bound molecules, whereas the fast one corresponded to that of the intracellular pool. When detected from outside by an Alexa488-conjugated anti-Thy1 Fab fragment, the lateral mobility of Thy1 showed a similar single long relaxation time to the longest one observed in the case of GFP-Thy1 (with a spot radius of ~240 nm, these times were 31.8 ± 5.8 and 27.4 ± 2.9 ms, respectively).

The FCS diffusion laws were then analyzed (Figure 3C). In the case of the two GPI-anchored proteins, GFP-Thy1 and GFP-GPI, t_0 was found to be significantly positive (18.4 ± 1.7 and 12.1 ± 2.5 ms, respectively), whereas the reverse was observed with the TfR-GFP, which gave a t_0 value of -20.4 ± 1.9 ms. Interestingly, the DPP_{IV}-GFP diffusion behavior was in between that observed with the GPI-anchored proteins and the TfR-GFP. The reason for this small positive intercept (4.8 ± 1.7 ms) will be discussed below.

In order to check whether the diffusion behavior reflected in the FCS corresponded to a significant fraction of the molecules tested, confocal FRAP measurements (Kenworthy *et al*, 2004) were performed. The mobile fraction M_f was assessed in terms of the percentage of the fluorescent molecules recovered in the bleached area during the FRAP experiment. All the lipid analogs were nearly 100% mobile, and $M_f > 95\%$ with FL-PC, FL-SM and FL-G_{M1}. In the case of the GFP-tagged proteins, the M_f value ranged between 77 and 92% (77, 85, 90 and 92% with TfR-GFP, DPP_{IV}-GFP, GFP-GPI and GFP-Thy1, respectively). The FCS diffusion laws given

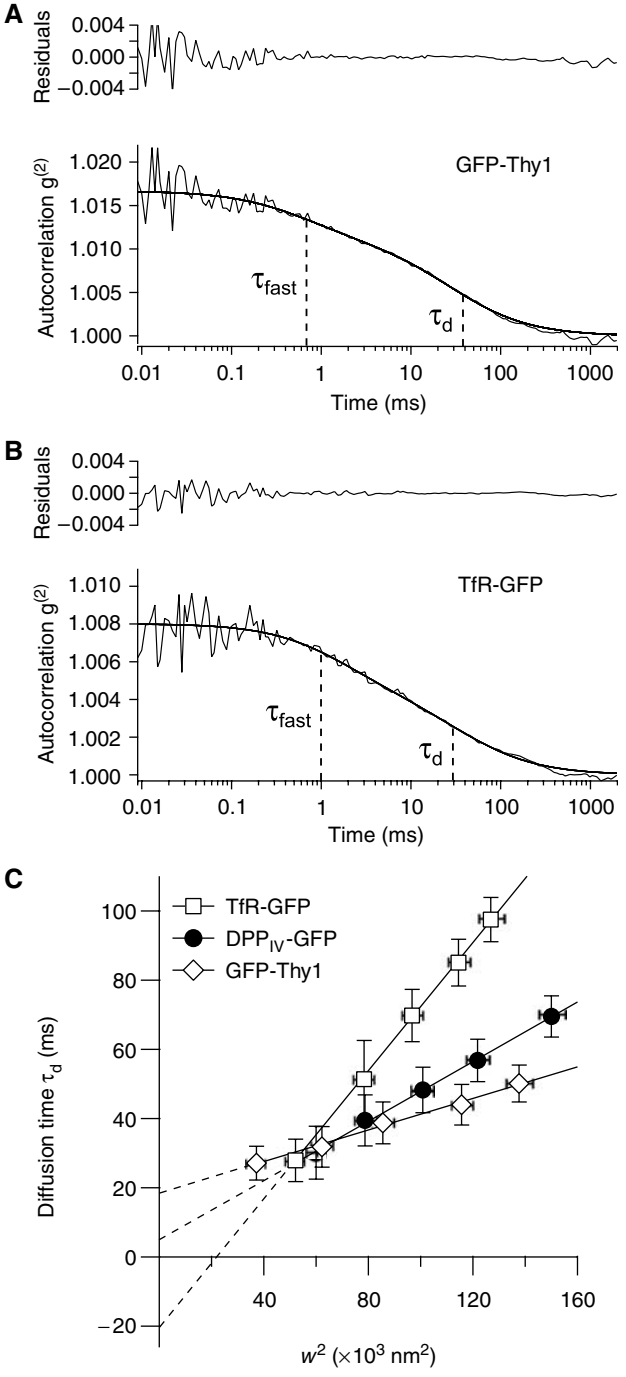

Figure 3 Diffusion behavior of GFP-tagged proteins. ACFs obtained with GFP-Thy1 (**A**) and TfR-GFP (**B**). In both cases, two decay times were clearly identified with the various probes used: a short time τ_{fast} and a longer one τ_d. (**C**) FCS diffusion laws in the case of TfR-GFP, DPP_{IV}-GFP and GFP-Thy1. Error bars on the *x* and *y* axes give the s.d.s of the means.

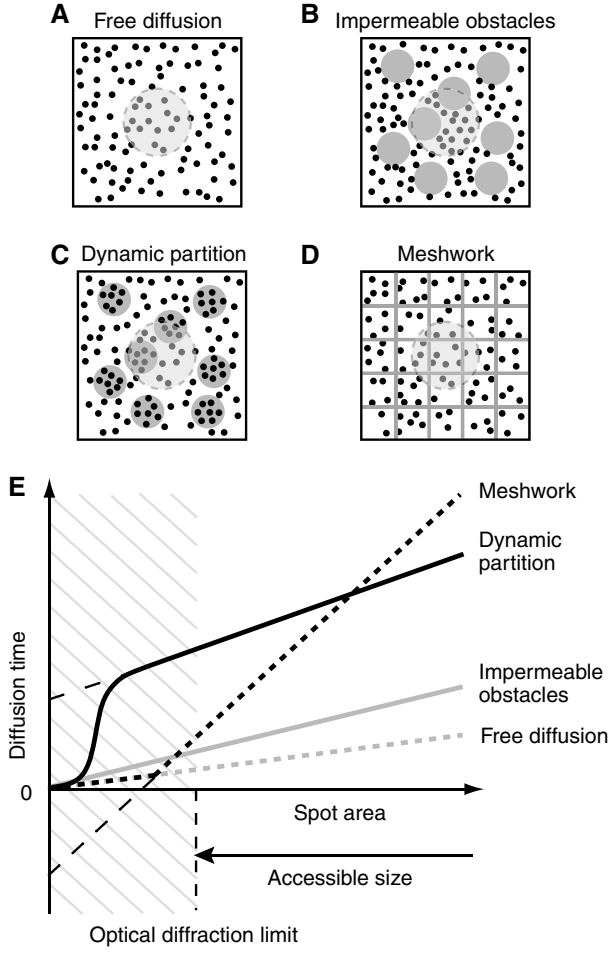

Figure 4 Simulated FCS diffusion laws corresponding to different membrane models. (A–D) Diffusion models for membrane organization. (**A**) In the free diffusion model, fluorescent molecules (black dots) show pure Brownian motion and fluoresce under the laser excitation spot (large gray circle). (**B**) In the presence of impermeable obstacles (gray spots), the diffusion is restricted to the free space. (**C**) When the domains are permeable (as the result of dynamic partition processes), the molecules can diffuse into and out of the microdomains and be transiently trapped (gray spots). (**D**) In a meshwork model, multiple adjacent domains are separated by barriers (gray lines) preventing the diffusion of the molecules. (**E**) Characteristic diffusion laws obtained for the different models. The diffusion time τ_d was analyzed as a function of the squared radius w^2. Diffusion laws applying to the free diffusion model (dotted gray curve), the diffusion process in the presence of impermeable obstacles (gray curve), the dynamic partition model (dotted black curve) and the meshwork model (black curve). Diffusion laws cannot be determined experimentally below the diffraction limit. For detailed analyses, see the Supplementary data and Wawrezinieck *et al* (2004, 2005).

above therefore accurately describe the behavior of a very large fraction of the lipid analogs and GFP-tagged proteins.

A broad range of t_0 values was obtained with the various molecules used to explore the occurrence of domains in the plasma membrane. Based on this parameter, three subsets of molecules were identified: the glycerophospholipid analogs (null t_0), the sphingolipid and GPI-anchored protein groups (positive t_0) and the transmembrane TfR-GFP (negative t_0).

In view of the above data and the results of our previous numerical simulations (Wawrezinieck *et al*, 2005), where the change in the sign of the *y*-intercept t_0 was correlated with different modes of membrane compartmentalization, we hypothesized that simple confinement models would explain the deviations from free diffusion (Figure 4; see also the Supplementary data). A positive t_0 was linked, for example, to the dynamic partition model, which may provide a basis for explaining the diffusion behavior of the sphingolipid and GPI-anchored protein groups, whereas with a negative t_0, TfR molecules may be subjected to membrane confinement due

to meshwork effects. Lastly, because of the null t_0, the glycerophospholipid analogs may neither be confined within discrete domains nor be hindered by a meshwork.

A lipid-dependent microdomain organization confines sphingolipid analogs and GPI-anchored proteins within the plasma membrane of resting cells

Among the mechanisms possibly responsible for confinement in discrete microdomains, several lines of evidence combine to support the idea that cholesterol and sphingomyelin are involved in the control and the organization of local heterogeneities: the differential packing characteristics of glycerophospholipids and sphingolipids with cholesterol promote the formation of a liquid-ordered phase or a similar state, which coexists in the membrane plane with a liquid-disordered phase (Brown and London, 1998; Rietveld and Simons, 1998). To test whether this hypothesis holds in the case of sphingolipid analogs and GPI-anchored proteins, cells were incubated in the presence of exogenous cholesterol oxidase (COase) or sphingomyelinase (SMase) to decrease the cholesterol and sphingomyelin membrane contents, respectively.

With 1 U/ml of COase, $23.3 \pm 2.2\%$ of the total cell cholesterol was converted into cholestenone. The ability of GPI-anchored proteins and sphingolipid analogs to float to the buoyant fractions of a sucrose gradient was subsequently found to be severely impaired (Figure 5A), and the FL-SM and FL-G_{M1} present in DRMs, as measured by spectrofluorimetry, decreased by 58 and 63%, respectively. This decrease in the cholesterol levels also induced significant changes in the behavior of GFP-GPI, since the curve of the corresponding FCS diffusion law then intercepted the time origin (0.2 ± 0.8 ms) (Figure 5B). Similar results were obtained with GFP-Thy1 and the sphingolipid analogs (Figures 5C, D

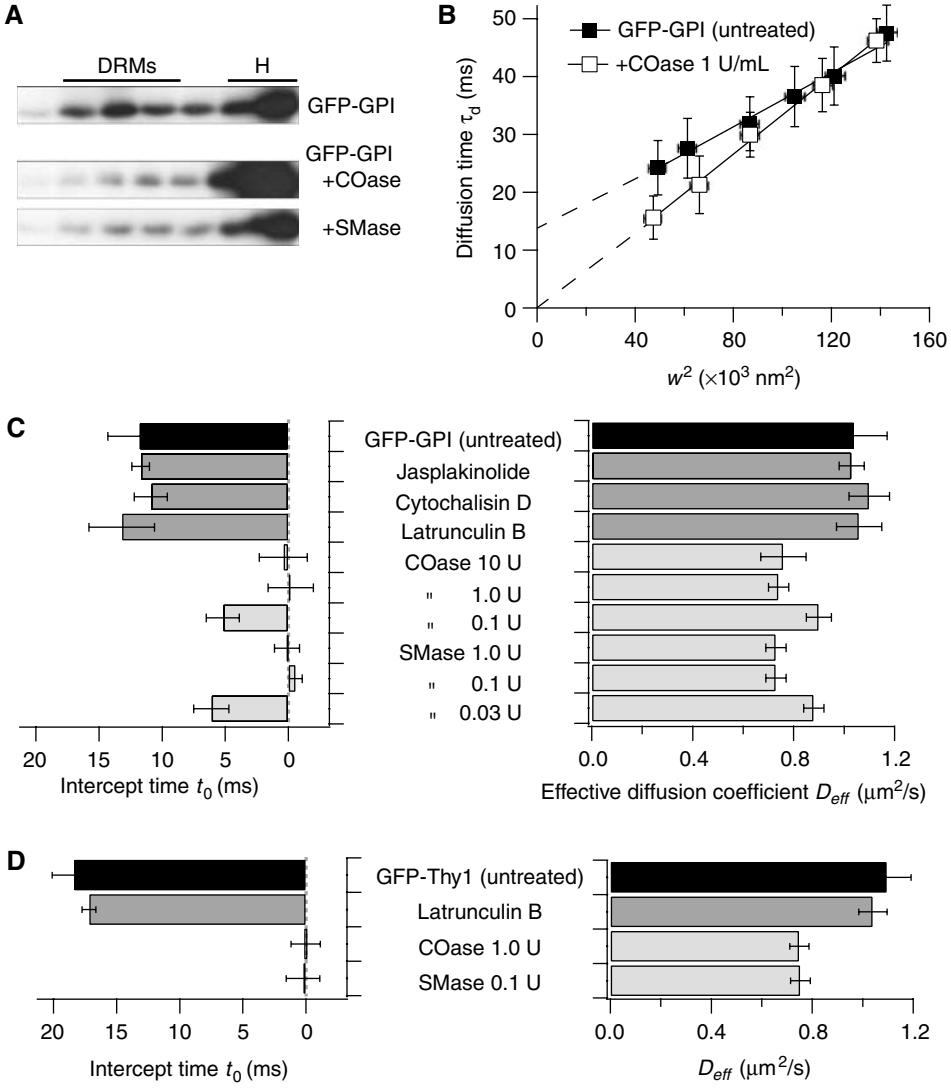

Figure 5 The confinement of GFP-tagged GPI-anchored proteins in microdomains is lipid-dependent. (**A**) Biochemical determination of GFP-GPI localization in DRMs after COase or SMase treatment. (**B**) FCS diffusion laws governing GFP-GPI proteins after cell treatment with COase. Error bars on the *x* and *y* axes are the s.d.s of the means. (**C**) Time intercept t_0 and effective diffusion coefficient D_{eff} obtained with GFP-GPI in untreated COS-7 cells (black bars), after cytoskeleton drug treatments (dark gray bars) or lipid modifications (light gray bars). (**D**) Idem in the case of GFP-Thy1 protein.

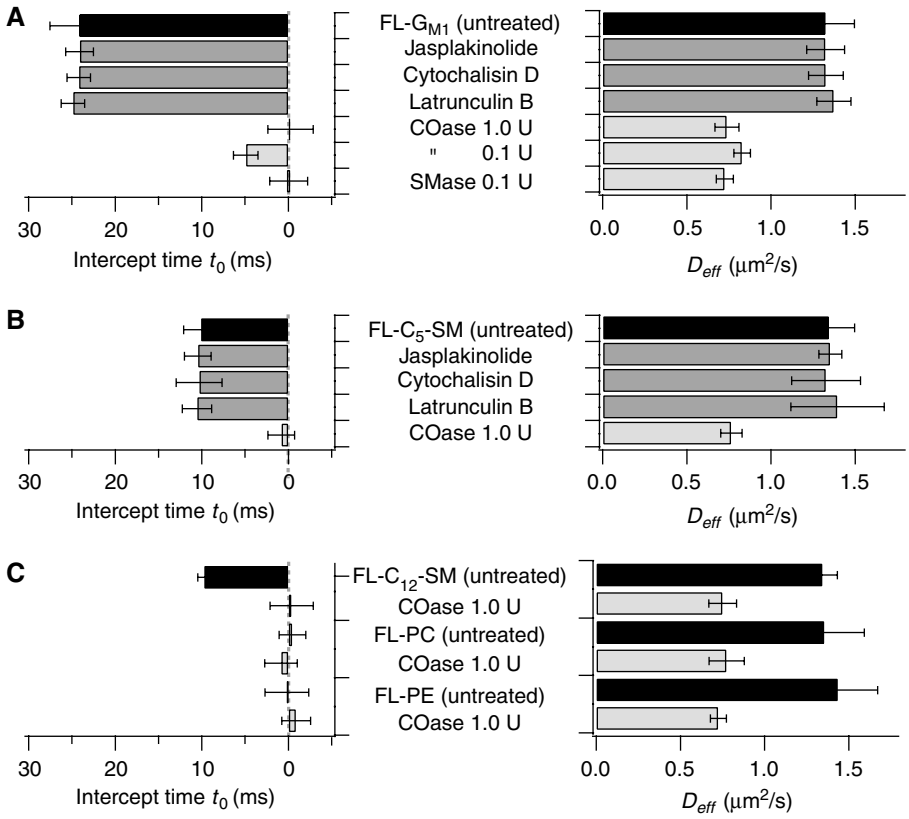

Figure 6 The confinement of lipid probes in the plasma membrane of COS-7 cells is lipid-dependent. Time intercept t_0 and effective diffusion coefficient D_{eff} obtained with FL-G$_{M1}$ (**A**), FL-C$_5$-SM (**B**) and the other lipid analogs used in this study (**C**) in untreated COS-7 cells (black bars), after applying cytoskeleton drug treatment (dark gray bars) or lipid modifications (light gray bars). Error bars give the s.d.s of the means.

and 6, respectively). Importantly, a 10-fold lower enzyme concentration, which converted $<10\%$ of the total cholesterol into cholestenone ($8.2\pm4.4\%$), led to an intermediate value between those obtained with cells treated and not with 1 U/ml of COase, as illustrated here in the case of GFP-GPI and FL-G$_{M1}$, (Figures 5C and 6A, respectively). The effects of the larger changes in the cholesterol content ($56.9\pm4.7\%$) induced by 10 U/ml of COase did not differ from those observed with 1 U/ml. All in all, these results suggest that the microdomain organization generated by dynamic partitioning processes no longer existed in these cell membranes.

We then hydrolyzed SM into ceramide by adding exogenous SMase to COS-7 cells. With 0.1 U/ml of SMase, $68\pm4\%$ of the total SM was hydrolyzed. At the same time, we noted that the presence of GFP-GPI within DRMs was also severely impaired after enzymatic treatment (Figure 5A). More importantly, the curves of all the FCS diffusion laws governing GFP-GPI, GFP-Thy1 and FL-G$_{M1}$ intercepted the time origin (Figures 5C–D and 6A). Once again, we observed that the SM membrane concentration was critical, since titration experiments showed that the confinement of GFP-GPI disappeared in a dose-dependent manner (Figure 5C). Lower concentrations (0.03 U/ml) converting $54\pm4\%$ of the total SM led to an intermediate value between those obtained with cells treated or not with 0.1 U/ml of SMase, as illustrated in the case of GFP-GPI and FL-G$_{M1}$. The effects of higher SMase concentrations (1 U/ml) did not differ from those observed with 0.1 U/ml.

It was remarkable that the lipid-mediated microdomain organization was entirely abolished when only $\sim20\%$ of the total cholesterol was converted into cholestenone by COase. This could be due to a combined effect of cholesterol hydrolysis and cholestenone production, since an antagonizing action of the cholestenone to ordered domains has been reported (Xu and London, 2000). A similar scenario might occur upon SMase treatment as well. Ceramide has recently been shown to displace cholesterol from sphingomyelin-cholesterol domains as well as to induce strong alterations of the lateral organization in model membranes (Megha and London, 2004).

After COase or SMase treatment, a similar decrease in D_{eff} occurred in both the GPI-anchored proteins and sphingolipid analogs ($\sim0.75\,\mu m^2/s$) (Figures 5 and 6). The fact that this was also the case with the glycerophospholipid analogs although the t_0 value was still null (Figure 6C) suggested that an overall change in the plasma membrane viscosity had also occurred due to the enzymatic change in the lipid membrane composition. All in all, these results strongly support the idea that in the absence of molecular crosslinking processes, sphingolipid analogs and GPI-anchored proteins are confined by a cholesterol and sphingomyelin-dependent process of microdomain formation.

A cytoskeleton-mediated meshwork hinders the lateral mobility of TfR-GFP

The TfR-GFP diffusion law curve, which showed a negative t_0, suggested that TfR molecules diffused in a meshwork

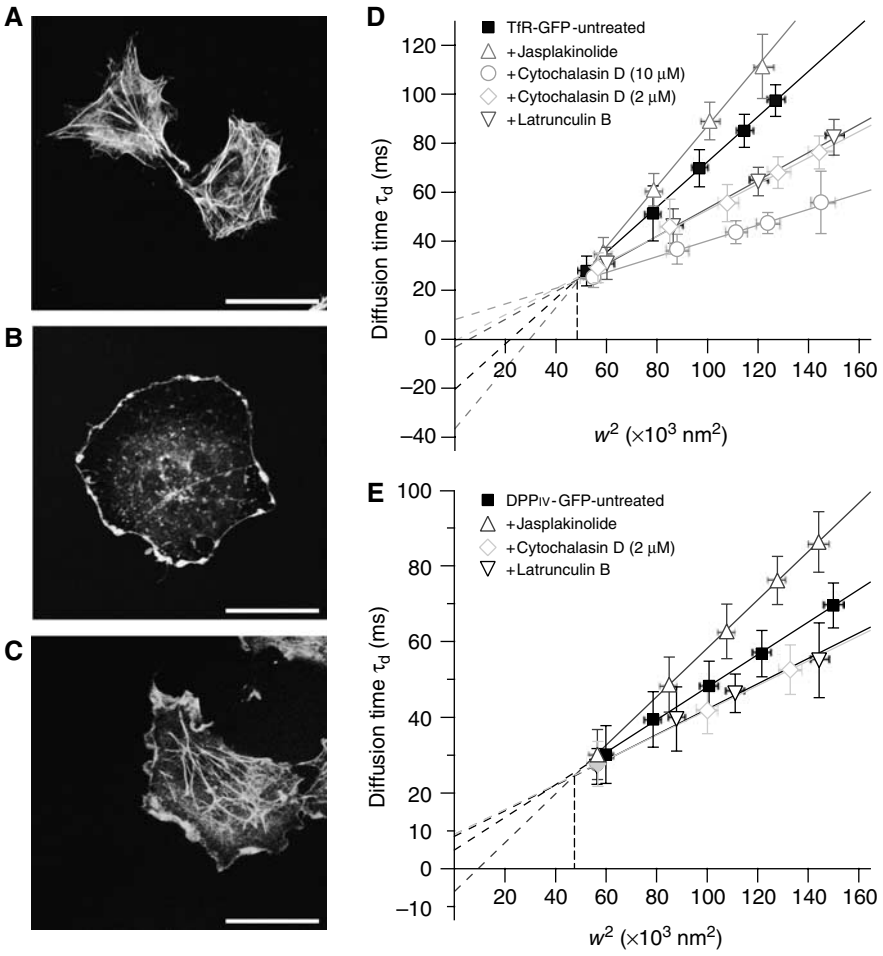

Figure 7 The GFP-tagged transmembrane protein diffusion laws are actin-dependent. Confocal images of rhodamine phalloidin labeling of F-actin in COS-7: (**A**) untreated; (**B**) 1 μM latrunculin B; (**C**) 0.4 μM jasplakinolide. Diffusion laws governing TfR-GFP (**D**) and DPP_{IV}-GFP (**E**) after applying cytoskeleton drug treatment. Error bars on the *x* and *y* axes are the s.d.s of the means.

context (Figure 4D and E). To investigate the possible involvement of the cytoskeleton, COS-7 cells were treated with drugs known to alter the actin-based cytoskeleton, such as latrunculin-B (an actin polymerization inhibitor), cytochalasin D (an actin depolymerization inducer) or jasplakinolide (an actin filament stabilizer). Suitable experimental conditions were first setup to ensure that these drugs changed the pattern of cytoskeleton organization without significantly affecting the cell morphology (Figure 7A–C).

The lateral mobility of TfR-GFP was then assessed (Figure 7D). Under latrunculin B (1 μM) or cytochalasin D (2 μM) treatment, the FCS diffusion law curve intercepted the *y*-axis near the time origin (-3.2 ± 1.8 and 0.7 ± 1.8 ms, respectively). These findings indicate that the physical barriers confining TfR-GFP were lowered. At the same time, the D_{eff} value increased from 0.27 ± 0.01 to $0.44 \pm 0.02\,\mu m^2/s$, which suggests that the long-range diffusion was less strongly impeded by the barriers between adjacent domains. Conversely, treatment with jasplakinolide (0.4 μM) decreased both the D_{eff} and t_0 values to $0.20 \pm 0.01\,\mu m^2/s$ and -36.5 ± 5.4 ms, respectively. This decrease suggests that the barriers confining TfR-GFP were reinforced by jasplakinolide treatment.

By contrast, it is noteworthy that neither the actin-based skeleton alterations induced by latrunculin B nor its stabilization by jasplakinolide had any effect on the molecular confinement observed with the GPI-anchored proteins and the sphingolipid analogs (Figures 5 and 6). Neither the t_0 nor D_{eff} values were affected under the experimental conditions that drastically altered the diffusion of TfR-GFP.

Meshwork and discrete domains contribute concomitantly to the dynamic compartmentalization of transmembrane proteins in the cell membrane

The shape of the diffusion law curve obtained for DPP_{IV}-GFP suggested that confinement by discrete domains may have occurred since, as observed in the case of GPI-anchored proteins, t_0 was positive. However, a similar study to that carried out on TfR-GFP showed that the FCS diffusion law was actin-dependent (Figure 7E). Treatment with latrunculin B or cytochalasin D led to increases in both t_0 and D_{eff}, whereas jasplakinolide treatment decreased both t_0 and D_{eff}, and even led to a negative t_0 value. More intriguingly, although TfR-GFP and DPP_{IV}-GFP were obviously sensitive to cytoskeleton-based compartmentalization, the possibility that discrete domain confinement may have occurred was

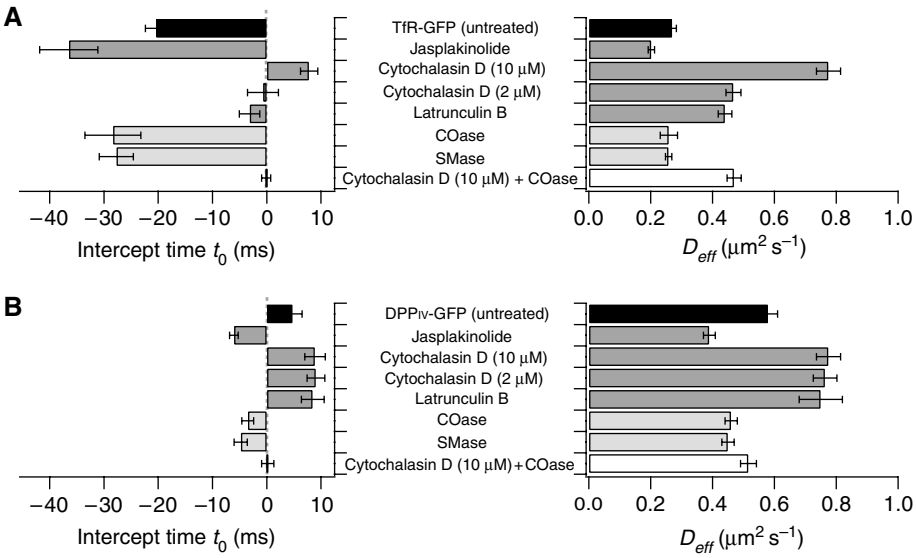

Figure 8 Both actin meshwork and lipid domains contribute to transmembrane protein compartmentalization. Time intercept t_0 and effective diffusion coefficient D_{eff} obtained with TfR-GFP (**A**) and DPP_{IV}-GFP (**B**) in untreated COS-7 cells (black bars), after applying cytoskeleton drug treatment (dark gray bars), after lipid modifications (light gray bars) or combined treatment (open bars). COase and SMase concentrations were 1 and 0.1 U/ml, respectively. Error bars are the s.d.s of the means.

suggested by the fact that high drug concentrations (cytochalasin D 10 μM) disrupted the actin network organization and gave a t_0 of 7.8 ± 1.6 and 8.9 ± 1.9 ms, respectively. In addition, the lipid modifications induced by COase or SMase systematically decreased the respective t_0 values (Figure 8). These two findings suggest that both meshwork and isolated domains contributed simultaneously to the DPP_{IV}-GFP and TfR-GFP diffusion process. To test this hypothesis, we then established the corresponding FCS diffusion laws under experimental conditions where actin-based cytoskeleton barriers and cholesterol were simultaneously modified (Figure 8). Significantly, τ_d for DPP_{IV}-GFP and TfR-GFP was found to be linear in w^2. Thus, when both confinement forces were relaxed, these proteins recovered free-like diffusion behavior.

Our study also indicated that the microdomain and the meshwork confinement may mask each other in the FCS law analysis. Indeed, we could interpret the differences in the diffusion modes between TfR-GFP and DPP_{IV}-GFP in terms of the differential strength of the actin-based and lipid-dependent confinement processes. COase and SMase treatments both abolished the lipid-dependent confinement process but unraveled the cytoskeleton-dependent one, which was in turn abolished by cytochalasin D or latrunculin B (Figure 8). With these TfR-GFP and DPP_{IV}-GFP proteins, COase treatment decreased the t_0 values to -28.4 ± 5.2 and -3.5 ± 1.1 ms, respectively. It was therefore deduced that the confinement of the cytoskeleton was about eight times stronger with TfR-GFP than DPP_{IV}-GFP. On the opposite, upon impairing the actin network, it was observed that both proteins underwent an almost identical weak lipid-dependent microdomain confinement process (7.8 ± 1.6 and 8.9 ± 1.9 ms for TfR-GFP and DPP_{IV}-GFP, respectively). It seems likely that the effects of cytoskeleton and lipid confinement may have been additive, but this hypothesis remains to be confirmed in further studies. The actin-based confinement process was stronger than the lipid-dependent one in the case of TfR-GFP, whereas the reverse was true in that of DPP_{IV}-GFP.

Discussion

The present study describing the diffusion behavior of diverse membrane components provides insights on the role of lipids in compartmentalizing the cell membrane. First, based on FCS data obtained on various spatial scales, we established that the sphingolipid analogs and GPI-anchored proteins undergo transient confinements in isolated microdomains. Secondly, the molecular origin of these confinement processes was found to be cholesterol- and sphingomyelin-dependent. Thirdly, their compartmentalization in isolated domains is independent of the actin-based cytoskeleton organization. Lastly, when the actin-based cytoskeleton confinement processes are relaxed, the contribution of lipid-dependent microdomains to confining transmembrane proteins was also readily observed. Overall, our data provide strong evidence supporting the idea that in live cells, a lipid-dependent microdomain organization is responsible for the dynamic molecular confinement of membrane components.

FCS diffusion laws provide a robust experimental frame of analysis for investigating the presence of submicron domains in live cells

Among the methods used to characterize the cell membrane, our novel experimental approach constitutes a significant advance, since it can be used to quantify relevant parameters to explore domain structure in the plasma membrane. Although FRAP and FCS methods involve similar experimental setups, the FCS method provides unique information, mainly because it combines high temporal resolution with single molecule sensitivity and robust statistical analysis (Schwille *et al*, 1999; Bacia *et al*, 2004). By comparison, the FRET methods frequently used to study membrane domains probe direct molecular interactions (Kenworthy and Edidin, 1998; Sharma *et al*, 2004), but these methods are not appropriate for studying long-range interactions and diffusive processes. SPT certainly competes with FCS, since it can be used to determine particle positions to within tens of nm and

in some cases, with a high temporal resolution (Schutz *et al*, 2000; Fujiwara *et al*, 2002). However, accurate interpretation of the SPT results generally requires analyzing large numbers of individual trajectories. Besides, in our FCS experiments, the direct conjugation of the fluorophore on the tracked molecules circumvents unwanted crosslinking and aggregation. Overall, the FCS approach described here for recording measurements on different spatial scales provides a highly appropriate means of exploring domain structure and dynamics in the plasma membranes of live cells.

The diffusion behavior of different subclasses of membrane components was determined here experimentally. Although the sphingolipid analogs show a lower affinity for DRMs than their natural counterparts (our data and Kuerschner *et al*, 2005), they are still useful to probe lipid raft organization, since FCS is sufficiently sensitive to be able to detect even small amounts of the fluorescent molecules in the coexisting phase (Korlach *et al*, 1999). The wide range of time intercepts t_0 measured (from -20 to $+20$ ms) suggests that different mechanisms may hinder the diffusion of membrane components. Based on our previous simulations (Wawrezinieck *et al*, 2005), these findings indicated that a strictly positive time intercept t_0 resulted from confinement into isolated domains, whereas a strictly negative value reflected the presence of a meshwork. It is significant that the components thought to be associated with lipid rafts, such as GPI-anchored proteins or sphingolipid analogs, showed strictly positive time intercepts, which suggests that a dynamic process of molecular partition into discrete domains mainly hinders their diffusion. By contrast, barriers predominantly impede the diffusion of the TfR-GFP since t_0 was strictly negative. Owing to the null t_0, the glycerophospholipid analogs apparently underwent unhindered diffusion.

Evidence supporting a lipid-dependent microdomain organization in live cells

A clearly visible signature of lipid-dependent compartmentalization is provided by COase and SMase enzymatic treatments. Our finding is consistent with previous data showing that both cholesterol and SM make a pivotal structural contribution to order domain formation (Brown and London, 1998; Rietveld and Simons, 1998). These results indicate that the lipid-dependent microdomain organization dictates the overall mobility of sphingolipid analogs and GPI-anchored proteins. It is also worth pointing out that the microdomains detected in the present study do actually exist in the plasma membrane of cells under steady-state conditions. This observation is in line with recently published data showing that phase separation and the formation of lipid domains do in fact occur in live cells (Meder *et al*, 2006).

Although an actin-based system of cytoskeleton compartmentalization has been described in the case of molecules located in the outer leaflet of the plasma membrane (Sako and Kusumi, 1994; Fujiwara *et al*, 2002; Kusumi *et al*, 2005), no such system was observed here in the mode of confinement of GPI-anchored proteins or sphingolipid analogs. Indeed, although cholesterol and SM modifications completely abolished the membrane confinement for these molecules, neither the actin-based cytoskeleton disorganization nor its stabilization had any such effects. Further studies are now required to determine whether the above discrepancies may be attributable to differences in the cell types, experimental conditions or techniques used. Our results are nevertheless in agreement with those of SPT analyses performed on GPI-anchored MHC class I and DiI molecules (Vrljic *et al*, 2005) as well as with the finding that cholesterol and/or SM modifications reduced the molecular mobility (Kenworthy *et al*, 2004; Nishimura *et al*, 2005; Vrljic *et al*, 2005).

The free diffusion behavior observed in the case of the glycerophospholipid analogs is similar to that previously observed in the case of Cy3-DOPE in the plasma membrane of various cell types at a recording rate of 100 ms/frame (Fujiwara *et al*, 2002; Kusumi *et al*, 2005). However, we were unable to detect any submicron-sized compartments such as those previously observed by authors performing SPT at an enhanced time resolution (25 μs/frame) using gold-tagged Cy3-DOPE molecules to label COS-7 cells (Kusumi *et al*, 2005).

A lipid-dependent microdomain organization also impedes the diffusion of transmembrane proteins

Our data clearly confirm the existence of fences confining transmembrane proteins, even if these molecules are not interacting directly with the cytoskeleton. For instance, the motion of TfR-GFP is mainly controlled by the actin-based membrane skeleton fences, and t_0 decreased when this meshwork was strengthened. It is also worth noting that all these experimental FCS diffusion laws form a bundle of lines with a common crossover point (Figure 7D). Previous simulations have shown that (i) these lines intersect at a single point in the meshwork at different barrier strengths but with the same mesh sizes; (ii) the crossover occurs when the spot area is about one to twice that of the mesh. Since the experimental crossover was obtained with $w^2 = 5 \times 10^4 \pm 1 \times 10^4\,\mathrm{nm}^2$, the area of the mesh was around $8 \times 10^4 \pm 2 \times 10^4\,\mathrm{nm}^2$. Assuming a square mesh, its sides would measure 240 ± 60 nm: this value is in good agreement with the 260 nm mesh size measured in rat kidney fibroblasts, which was determined by SPT experiments performed at 25 μs/image (Fujiwara *et al*, 2002). However, in our case, we did not detect any enlarged meshes after a partial disruption of the cytoskeleton. In addition, we observed that a treatment by cytochalasin D at 10 μM released TfR-GFP and DPP_{IV}-GFP proteins from the meshwork-based state of confinement. Nevertheless, the latter proteins still underwent the lipid domain-based constrained diffusion on a much smaller compartmentalization scale.

Some extremely interesting features have been brought to light by monitoring the motion of these proteins after subjecting them to treatments that disrupt the actin-based cytoskeleton and/or decrease the membrane cholesterol level. This combined treatment applied here induced the recovery of an FCS diffusion law curve, which intercepted the time origin. A single treatment abolishing one of the two major hindrance mechanisms served to show up the other one.

Main features of lipid-dependent microdomains

Our observations of the sphingolipid and cholesterol dependency for the lipid-dependent microdomains revealed by the FCS diffusion study suggest that they correspond to lipid rafts, a type of microdomains proposed to be involved in numerous cellular functions, but whose existence has been matter of controversy. The current view is that 'membrane

rafts are small (10–200 nm), heterogeneous, highly dynamic, sterol- and sphingolipid-enriched domains that compartmentalize cellular processes' (Pike, 2006). The analysis of our experimental data in the light of the simulation studies allow us to further conclude that the lipid-mediated microdomains described here fit the above description very nicely in many respects.

As mentioned above, our FCS method is sensitive to nanoscale confining structures. Based on dynamic molecular partition simulations, we were able to determine the upper limit of the microdomain radius r (Supplementary Figure S1). We previously observed that the graph line between τ_d and w^2 is solely observed if the observation spot is significantly larger than the domains ($w^2/r^2 > 10$ in the case of isolated microdomains) (Wawrezinieck *et al*, 2005). In our experiments, the smallest observation spot was close to the transverse resolution limit of the microscope ($\sim$200 nm); the upper limit of the microdomain radius r is therefore around 60 nm: this value is consistent with data published in the literature (Pralle *et al*, 2000; Zacharias *et al*, 2002; Prior *et al*, 2003; Sharma *et al*, 2004).

The t_0 intercept could be of special interest, since it could be used to delineate the temporal characteristics of these microdomains. In the simulation models, this value depends on both the partition factor α of a given molecule in the microdomains and the confinement time within one microdomain τ_{conf} (see equation (2) in the Supplementary data). The value of α is not yet available, but based on DRM experiments, we might tentatively take this value to range between 10 and 30%. For instance, with a t_0 value of 18.4 ms in the case of GFP-Thy1, we have 31 ms $< (\tau_{conf} - \tau_d^{domain}) <$ 92 ms. Since we measured that $\tau_d > 30$ ms when $(w/r)^2 > 10$, the diffusion time in a domain should be at most 30/10 $\sim$ 3 ms. It can therefore be concluded that τ_{conf} ranges between 34 and 95 ms. Confinement in microdomains is therefore an extremely transient process taking probably only some tens to hundreds of milliseconds. Reaching a deeper understanding of t_0 obviously constitutes one of most important and challenging issues awaiting future theoretical analysis. Our experiments showed (Figures 5 and 6) that before reaching the maximum effect (i.e. $t_0 \sim$ null), a parallel existed between the change in the sphingomyelin or cholesterol levels and the decrease in t_0. It is therefore possible to consider this parameter as a *microdomain confinement index,* since the partition factor α and the confinement time τ_{conf} are essential parameters characterizing the confinement into microdomains.

We would like to stress the fact that our results do not tell us whether membrane molecules partition dynamically into pre-existing raft domains or whether they directly participate in assembly/disassembly of the domains forming self-promoting membrane complexes. This is because the confinement time τ_{conf} is always to be either shorter than or equal to the lifetime of the microdomain in our models. In the first case, the molecule is partitioning dynamically into a pre-existing domain, whereas in the second case, the molecule accompanies/participates in the assembly and disassembly of the domain. In the same context, we observed in our FCS measurements that the diffusion time τ_d remained constant within the limits of the experimental error bars although the amount of fluorescent probe used varied by a factor of 20 (i.e. from $\sim$100 to $\sim$2000 μm^{-2} in the case of GFP-GPI) (Supplementary Figure S2). Consequently, the probe concentration does not greatly affect the diffusion behavior of the probe. However, this is not relevant to the question as to whether we are dealing with pre-existing or self-assembling raft models, because our FCS analysis did not include the probe density, contrary to recent FRET and immuno-EM studies on nanoscale membrane organization (Sharma *et al*, 2004; Hess *et al*, 2005; Plowman *et al*, 2005).

Overall, our data strongly support a dynamic picture where nanometer-scale microdomains confine constituents for up to a few tens to hundreds of milliseconds and undergo continuous changes as molecular diffusion processes occur. These findings also show that studies on diffusion behavior throw particularly useful light on the modes of lateral membrane organization, which are likely to be largely governed by weak molecular interactions.

Materials and methods

DNA constructs and cell transfection procedures

GFP-GPI was provided by A LeBivic (IBDM, Marseille, France). DPP_{IV}-GFP was obtained from G Trugnan (INSERM, Paris, France). The human TfR cDNA was provided by S Méresse (CIML, Marseille, France). The Thy1 gene expression vector and the Alexa488-conjugated anti-Thy1 Fab fragment were a kind gift from R Morris (King's College London, UK). To construct GFP-Thy1, three overlapping fragments were PCR amplified and cloned into the pEGFP-C1 plasmid. This yielded a recombinant GFP-Thy1 cDNA encoding the 19th aa of Thy1 (signal peptide), the EGFP and the remaining sequence of Thy1 (aa 20–162). To construct TfR-GFP, the TfR cDNA (aa 1–112) was cloned inframe with the GFP cDNA into the pEGFP-N3 plasmid.

All experiments were carried out on COS-7 cells (ATCC, CRL-1657). Cells were grown in DME supplemented with 10% FCS, glutamine and sodium pyruvate. Transient transfections were performed with ExGen 500 as per the manufacturer's instructions (Euromedex) and 24 h before FCS measurements.

Fluorescent staining with lipid analogs

Complexes of BODIPY-lipids (Invitrogen) and BSA were prepared in line with the manufacturer's instructions and as described in Martin and Pagano (1994). Briefly, 500 nmol of FL-SM or FL-GM1 stock solution ($CHCl_3$:MeOH 19:1) were dried under a stream of nitrogen, and then under a vacuum for at least 1 h. The dried lipid was dissolved in 200 µl of absolute ethanol and injected into 10 ml of defatted BSA solution (5 µM defatted BSA in Hanks buffered salt solution containing 10 mM HEPES pH 7.4, HBSS/HEPES) while vortexing vigorously. FL-PC and FL-PE were prepared in a similar way, except that the lipid to BSA ratio was 2:1 (mol:mol). Cell cultures were washed in HBSS/HEPES, incubated with 0.05 µM lipid/BSA complex in HBSS/HEPES for 30 min at 4°C, washed and further incubated in HBSS/HEPES at 37°C.

Treatment of cells with enzymes and drugs

To modify the cholesterol or sphingomyelin contents of plasma membrane, cells were treated with *Streptomyces* sp. COase or *Staphylocuccus aureus* SMase (Calbiochem) in serum-free HBSS/HEPES buffer at 1 U/ml for 30 min or at 0.1 U/ml for 5 min, respectively. Cells were washed in HBSS/HEPES prior to the diffusion measurements. Prior to pharmacological treatments, cells were washed in HBSS/HEPES and incubated at 37°C with 1 µM latrunculin B (5 min), 2–10 µM cytochalasin D (30 min) or 0.4 µM jasplakinolide (5 min). All FCS measurements were completed within 30 min of the cell treatment, before any significant morphological changes in the cell could take place.

Biochemical analyses

To determine the cholesterol levels, cells were scraped off and lyzed at 4°C for 30 min in a buffer containing 1% Nonidet P-40, 10 mM Tris pH 7.4, 150 mM NaCl, 1 mM EDTA and protease inhibitors. Samples were cleared by centrifugation at a rate of 12 000 *g* before

undergoing fluorometric measurements using the Amplex®Red Cholesterol kit (Invitrogen).

To determine the sphingomyelin levels, a similar procedure was used, except that the cells were lyzed at 4°C by sonication and the PNS harvested by centrifugation. Lipid extraction was performed using the Bligh–Dyer method (Bligh and Dyer, 1959) and the sphingomyelin levels were determined using a fluorometric method with the Amplex®Red sphingomyelinase assay kit (Invitrogen) as described in He *et al* (2002). With each test sample, a negative control assay was run on the sample and the reaction mixture devoid of SMase. Sphingomyelin amounts were calculated from the difference in fluorescence between the test and control samples, and compared with a standard.

To isolate DRMs, Brij98 (1%) solubilized postnuclear supernatant was fractionated on the sucrose gradient by centrifugation at 38 000 r.p.m. for 16 h in a SW41 rotor (Beckman Instruments Inc.) (Drevot *et al*, 2002). Fractions were resolved on SDS–PAGE and blotted with anti-GFP mAbs (Roche Molecular Biochemicals). The presence of DRMs was monitored, based on the distribution of Rab5 and ganglioside G_{M1} over the sucrose gradient. Spectrofluorimetry measurements were performed on the different fractions of the lipid analogs.

Fluorescence microscopy, FCS measurements and numerical analysis

Details of the experimental fluorescence microscopy, FRAP, FCS and numerical analysis procedures used are given in the Supplementary data, as well as in previous studies (Kenworthy *et al*, 2004; Wawrezinieck *et al*, 2004, 2005).

Supplementary data

Supplementary data are available at *The EMBO Journal* Online.

Acknowledgements

We thank R Morris, M Edidin, A Lellouch and P Golstein, for helpful discussions and suggestions and for critically reviewing the manuscript, J Blanc for editing the English. R Morris, A LeBivic, G Trugnan and S Méresse generously provided reagents and the use of the PICsL imaging core facility and technical assistance. This research was supported by institutional grants from INSERM and CNRS, and by specific grants from FRM, MENRT, EU FEDER and CNRS. LW and FC have been awarded fellowships from the MENRT.

References

Bacia K, Scherfeld D, Kahya N, Schwille P (2004) Fluorescence correlation spectroscopy relates rafts in model and native membranes. *Biophys J* **87:** 1034–1043

Bligh EG, Dyer WJ (1959) A rapid method of total lipid extraction and purification. *Can J Biochem Physiol* **37:** 911–917

Brown DA, London E (1998) Functions of lipid rafts in biological membranes. *Annu Rev Cell Dev Biol* **14:** 111–136

Drevot P, Langlet C, Guo XJ, Bernard AM, Colard O, Chauvin JP, Lasserre R, He HT (2002) TCR signal initiation machinery is preassembled and activated in a subset of membrane rafts. *EMBO J* **21:** 1899–1908

Edidin M (2003) The state of lipid rafts: from model membranes to cells. *Annu Rev Biophys Biomol Struct* **32:** 257–283

Fujiwara T, Ritchie K, Murakoshi H, Jacobson K, Kusumi A (2002) Phospholipids undergo hop diffusion in compartmentalized cell membrane. *J Cell Biol* **157:** 1071–1081

Gaus K, Gratton E, Kable EP, Jones AS, Gelissen I, Kritharides L, Jessup W (2003) Visualizing lipid structure and raft domains in living cells with two-photon microscopy. *Proc Natl Acad Sci USA* **100:** 15554–15559

He X, Chen F, McGovern MM, Schuchman EH (2002) A fluorescence-based, high-throughput sphingomyelin assay for the analysis of Niemann–Pick disease and other disorders of sphingomyelin metabolism. *Anal Biochem* **306:** 115–123

Hess ST, Kumar M, Verma A, Farrington J, Kenworthy A, Zimmerberg J (2005) Quantitative electron microscopy and fluorescence spectroscopy of the membrane distribution of influenza hemagglutinin. *J Cell Biol* **169:** 965–976

Kenworthy AK, Edidin M (1998) Distribution of a glycosylphosphatidylinositol-anchored protein at the apical surface of MDCK cells examined at a resolution of <100 A using imaging fluorescence resonance energy transfer. *J Cell Biol* **142:** 69–84

Kenworthy AK, Nichols BJ, Remmert CL, Hendrix GM, Kumar M, Zimmerberg J, Lippincott-Schwartz J (2004) Dynamics of putative raft-associated proteins at the cell surface. *J Cell Biol* **165:** 735–746

Korlach J, Schwille P, Webb WW, Feigenson GW (1999) Characterization of lipid bilayer phases by confocal microscopy and fluorescence correlation spectroscopy. *Proc Natl Acad Sci USA* **96:** 8461–8466

Kuerschner L, Ejsing CS, Ekroos K, Shevchenko A, Anderson KI, Thiele C (2005) Polyene-lipids: a new tool to image lipids. *Nat Methods* **2:** 39–45

Kusumi A, Ike H, Nakada C, Murase K, Fujiwara T (2005) Single-molecule tracking of membrane molecules: plasma membrane compartmentalization and dynamic assembly of raft-philic signaling molecules. *Semin Immunol* **17:** 3–21

Marguet D, Lenne PF, Rigneault H, He HT (2006) Dynamics in the plasma membrane: how to combine fluidity and order. *EMBO J* [E-pub ahead of print: 22 June 2006; doi:10.1038/sj.emboj.7601204]

Marguet D, Spiliotis ET, Pentcheva T, Lebowitz M, Schneck J, Edidin M (1999) Lateral diffusion of GFP-tagged H2Ld molecules and of GFP-TAP1 reports on the assembly and retention of these molecules in the endoplasmic reticulum. *Immunity* **11:** 231–240

Martin OC, Pagano RE (1994) Internalization and sorting of a fluorescent analogue of glucosylceramide to the Golgi apparatus of human skin fibroblasts: utilization of endocytic and nonendocytic transport mechanisms. *J Cell Biol* **125:** 769–781

Meder D, Moreno MJ, Verkade P, Vaz WL, Simons K (2006) Phase coexistence and connectivity in the apical membrane of polarized epithelial cells. *Proc Natl Acad Sci USA* **103:** 329–334

Megha, London E (2004) Ceramide selectively displaces cholesterol from ordered lipid domains (rafts): implications for lipid raft structure and function. *J Biol Chem* **279:** 9997–10004

Munro S (2003) Lipid rafts: elusive or illusive? *Cell* **115:** 377–388

Nishimura SY, Vrljic M, Klein LO, McConnell HM, Moerner WE (2005) Cholesterol depletion induces solid-like regions in the plasma membrane. *Biophys J* **90:** 927–938

Pike LJ (2006) Rafts defined. *J Lipid Res* [E-pub ahead of print: 27 April 2006; doi:10.1194/jlr.E600002-JLR200]

Plowman SJ, Muncke C, Parton RG, Hancock JF (2005) H-ras, K-ras, and inner plasma membrane raft proteins operate in nanoclusters with differential dependence on the actin cytoskeleton. *Proc Natl Acad Sci USA* **102:** 15500–15505

Pralle A, Keller P, Florin EL, Simons K, Horber JK (2000) Sphingolipid-cholesterol rafts diffuse as small entities in the plasma membrane of mammalian cells. *J Cell Biol* **148:** 997–1008

Prior IA, Muncke C, Parton RG, Hancock JF (2003) Direct visualization of Ras proteins in spatially distinct cell surface microdomains. *J Cell Biol* **160:** 165–170

Rietveld A, Simons K (1998) The differential miscibility of lipids as the basis for the formation of functional membrane rafts. *Biochim Biophys Acta* **1376:** 467–479

Sako Y, Kusumi A (1994) Compartmentalized structure of the plasma membrane for receptor movements as revealed by a nanometer-level motion analysis. *J Cell Biol* **125:** 1251–1264

Saxton MJ (2005) New and notable: fluorescence corralation spectroscopy. *Biophys J* **89:** 3678–3679

Schutz GJ, Kada G, Pastushenko VP, Schindler H (2000) Properties of lipid microdomains in a muscle cell membrane visualized by single molecule microscopy. *EMBO J* **19:** 892–901

Schwille P, Haupts U, Maiti S, Webb WW (1999) Molecular dynamics in living cells observed by fluorescence correlation spectroscopy with one- and two-photon excitation. *Biophys J* **77:** 2251–2265

Sharma P, Varma R, Sarasij RC, Ira, Gousset K, Krishnamoorthy G, Rao M, Mayor S (2004) Nanoscale organization of multiple GPI-anchored proteins in living cell membranes. *Cell* **116:** 577–589

Shvartsman DE, Kotler M, Tall RD, Roth MG, Henis YI (2003) Differently anchored influenza hemagglutinin mutants display distinct interaction dynamics with mutual rafts. *J Cell Biol* **163:** 879–888

Simons K, Ikonen E (1997) Functional rafts in cell membranes. *Nature* **387:** 569–572

Simons K, Vaz WL (2004) Model systems, lipid rafts, and cell membranes. *Annu Rev Biophys Biomol Struct* **33:** 269–295

van Meer G (2005) Cellular lipidomics. *EMBO J* **24:** 3159–3165

Vrljic M, Nishimura SY, Moerner WE, McConnell HM (2005) Cholesterol depletion suppresses the translational diffusion of class II major histocompatibility complex proteins in the plasma membrane. *Biophys J* **88:** 334–347

Wawrezinieck L, Lenne P-F, Marguet D, Rigneault H (2004) Fluorescence correlation spectroscopy to determine diffusion laws: application to live cell membranes. *Proc SPIE* **5462:** 92–102

Wawrezinieck L, Rigneault H, Marguet D, Lenne P-F (2005) Fluorescence correlation spectroscopy diffusion laws to probe the submicron cell membrane organization. *Biophys J* **89:** 4029–4042

Xu X, London E (2000) The effect of sterol structure on membrane lipid domains reveals how cholesterol can induce lipid domain formation. *Biochemistry* **39:** 843–849

Yechiel E, Edidin M (1987) Micrometer-scale domains in fibroblast plasma membranes. *J Cell Biol* **105:** 755–760

Zacharias DA, Violin JD, Newton AC, Tsien RY (2002) Partitioning of lipid-modified monomeric GFPs into membrane microdomains of live cells. *Science* **296:** 913–916

